1992

Induction Motor Modeling Using Coupled Magnetic Field and Electric Circuit Equations

L. W. Marriott
Tecumseh Products Research Laboratory

G. C. Griner
Tecumseh Products Research Laboratory

INDUCTION MOTOR MODELING USING COUPLED MAGNETIC FIELD AND ELECTRIC CIRCUIT EQUATIONS

Lee W. Marriott Glenn C. Griner

Tecumseh Products Research Laboratory
3869 Research Park Drive
Ann Arbor, Michigan 48108
(313) 665-9182

ABSTRACT

Traditional design/prototype/test cycles have improved the efficiencies of small induction motors to high levels. To achieve still higher efficiencies, motor performance must be studied in a more detailed and integrated manner. The authors present a nonlinear, time-dependent computer simulaton modeling the performance of a permanent-split-capacitor induction motor. The effects of nonlinear permeability and time varying terminal voltages are included in the model. Two-dimensional finite element magnetic field equations are coupled with the electric circuit equations and solved using the Newton-Raphson and Crank-Nicholson methods. The simulation predicts main and auxiliary winding currents, induced rotor currents, hysteresis losses and motor torque as functions of time. Due to the detailed nature of the results a deeper understanding of motor performance factors, normally difficult to determine, can be obtained.

INTRODUCTION

Induction motor design involves the prediction and evaluation of performance parameters such as torque, line current and losses at any given slip and terminal conditions. These parameters can be accurately determined only with knowledge of the magnetic field distribution within the machine. Approximate analytical methods [1] have been used in the past with some success. Continued pressure to conserve energy dictates improved motor performance. This requires an even more detailed knowledge of the magnetic fields occurring within motors. Two-dimensional stationary magnetic field problems have been investigated by many authors [2,3]. The nonlinear permeability or saturation characteristics of steel require iterative methods for the solution of these problems. Tandon, Armor and Chari [4] were first to combine the Newton- Raphson technique with the Crank-Nicholson central difference scheme to solve transient field problems in electrical machines. The disadvantage of these methods is that they rely on apriori knowledge of the currents or current densities in the device.

The problem is much more complicated when current densities are unknown and terminal conditions must be considered. Potter and Cambrell [5] combined a two-dimensional finite element field solution and circuit equations to simulate an induction motor. In their work the stator field was replaced with a current sheet at slip frequency. Strangas and Theis [6] also combined the finite element field solution with circuit equations to model a shaded-pole motor. Their approach used a time-dependent grid for rotor movement. This paper expands the above techniques to model a permanent-split-capacitor induction motor. The two-dimensional magnetic field equations are combined with electric circuit equations describing end and external effects. The partial derivatives

of the combined system of equations form a Jacobian matrix which is solved by the Newton-Raphson method for each time step. Equilibrium at each time step is obtained when the derivatives of the time-dependent nonlinear magnetic field equations are satisfied. The electric circuit equations are linear ordinary differential equations appearing as constants in the Jacobian matrix. The solution advances through time by updating the time dependent terms of the Jacobian matrix and corresponding right hand side. The Crank-Nicholson finite difference method, being an implicit method, requires an inversion to solve for the unknowns in the next time step. This inversion is carried out by a complex math "sky-line" linear equation solver.

MAGNETIC FIELD EQUATIONS

The solution of the magnetic field problem is based on three of Maxwell's equations and the magnetic and electric field constitutive laws. Neglecting displacement current these equations are:

$$\nabla \times H = J \tag{1}$$

$$\nabla \times E = -\frac{\partial B}{\partial t} \tag{2}$$

$$\nabla \bullet B = 0 \tag{3}$$

$$H = \nu B \tag{4}$$

$$J = \sigma E \tag{5}$$

Where H is magnetic field intensity, B is magnetic flux density, E is electric field intensity, J is current density, ν is reluctivity and σ is an effective conductivity.

A vector potential function A is chosen such that the following relationship is satisfied:

$$\nabla \times A = B \tag{6}$$

Combining equations (1) through (6) and introducing the gradient of the scalar voltage as shown in [12], yields the time-dependent magnetic field equation:

$$\nabla \times (\nu \nabla \times A) = -\sigma \frac{\partial A}{\partial t} - \sigma \nabla V \tag{7}$$

FINITE ELEMENT APPROXIMATION OF THE MAGNETIC FIELD

The finite element method was employed to approximate the magnetic field equations. Many authors have contributed to this methodology. Some of the earliest magnetics work is attributed to Silvester and Chari [2]. The basic assumption of the method is that the vector potential within a finite element can be approximated by a linear combination of shape functions:

$$A\left(\xi,\eta\right) = \sum_{i=1}^{n} N_i\left(\xi,\eta\right) A_i \tag{8}$$

Where N_i are shape functions and n is the number of nodes in the element. Examples of shape functions may be found in the text books of Zienkiewicz [7] or Bathe [8]. Using this approximation and the minimization of the energy functional, the assembled finite element magnetic field equations become:

$$[T]\frac{\partial A}{\partial t}+[S(A)]A-[N_w]V_w-[N_b]V_b=0 \qquad (9)$$

Where $[T]$ is the global conductivity matrix, A is the global vector of vector potentials, $\frac{\partial A}{\partial t}$ is a vector of time derivatives of A, $S(A)$ is a nonlinear global coefficient matrix, $[N_w]$ is a matrix of weighting factors which distribute and convert coil voltages into element nodal current densities, V_w is the applied voltage across a length of coil lying within the lamination stack, $[N_b]$ is a matrix of weighting factors which distribute and convert rotor bar voltages into element nodal current densities and V_b is the applied voltage across a rotor bar length. The matrices and vectors given above are comprised of an assembly of element matrices, the details of which can be found in reference [12].

ELECTRIC CIRCUIT EQUATIONS

The electric circuit is characterized by two linear differential equations. The first equation sums the voltages along a rotor bar or coil and can be written as:

$$V_{applied}=V_{induced}-IR \qquad (10)$$

Where I is the current, V is voltage and R is a bar or effective coil resistance. The induced voltage along a length of a coil or rotor bar is:

$$V_{induced}=\frac{L}{A_c}\int\frac{\partial A}{\partial t}\,dS \qquad (11)$$

Substitution of the induced voltage (11) into equation (10), dividing through by the resistance and introducing $\frac{\partial A}{\partial t}$ as a vector of nodal vector potential time derivatives yields a first order differential equation which is coupled to the magnetic field equation (9).

$$-[N]\frac{\partial A}{\partial t}+\frac{\sigma A_c}{L}V-nI\bar{n}=0 \qquad (12)$$

Where $[N]$ is a matrix of Newton-Cotes integration factors, A_c is the area of a conductor, L is the length of the conductors, n is the number of conductors and $\bar{n}$ is a current direction vector for the winding.

It should be noted that this equation is dependent on the solution of the magnetic field equations for the values of $\frac{\partial A}{\partial t}$ and assumes that the applied voltage V is uniform across a coil or a rotor bar. The second equation is based on Kirchhoff's law as applied to a winding:

$$\Sigma nV\bar{n}+IR_e+L_e\frac{\partial I}{\partial t}+\frac{1}{C_{ext}}\int Idt=V_T(t) \qquad (13)$$

Where n is the number of conductors, V is the individual coil voltage, R_e is the end resistance, L_e is the end inductance, C_{ext} is the external capacitance, $\bar{n}$ is a direction vector, $V_T(t)$ is the time-dependent terminal voltage and Σ is a summation over the number of coils contributing to a winding. Notice that this equation is coupled to the first circuit equation (12) but does not directly influence the magnetic field equations. Note also that any other external impedances in series with the winding could be added to equation (13). Equations similiar to equations (12 and 13) can also be written for the rotor. Using the

method of rotor representation used by Strangas and Theis [6], rotor end ring currents and voltages are solved for rather than rotor bar voltages and currents. Rotor bar currents are then computed by summation of the appropriate end ring currents.

CRANK-NICHOLSON METHOD

The Crank-Nicholson method [9] is a numerically stable implicit central-difference scheme in which the basic assumption is:

$$A^{n+1} = A^n + \frac{\Delta t}{2}\left[\frac{\partial A^{n+1}}{\partial t} + \frac{\partial A^n}{\partial t}\right] \tag{14}$$

Combining equations (9), (12), (13) and (14) for the present (n) and future ($n+1$) time steps as shown in [12] yields the coupled finite difference magnetic field and electric circuit system of equations:

$$\begin{bmatrix} \nu[S] + \frac{2}{\Delta t}[T] & -\frac{\sigma}{L}[N_1] & 0 \\ -\frac{2}{\Delta t}\sigma[N_1]^T & \frac{\sigma A_c}{L} & -n\,\bar{n} \\ 0 & -n\,\bar{n} & -\left(Re + \frac{2}{\Delta t}Le + \frac{\Delta t}{2C_{ext}}\right) \end{bmatrix} \cdot \begin{Bmatrix} A^{n+1} \\ V^{n+1} \\ I^{n+1} \end{Bmatrix} =$$

$$\begin{bmatrix} \left[-\left[S(A) + \frac{2}{\Delta t}[T]\right]A^n\right] - [Nw]V_w^n - [N_b]V_b^n \\ \frac{2}{\Delta t}\sigma[N_1]^T A^n - \frac{\sigma A_c}{L}V^n + nI^n\,\bar{n} \\ -nV^n\,\bar{n} - \left(Re + \frac{2}{\Delta t}Le + \frac{\Delta t}{2C_{ext}}\right)I^n + V_T^{n+1} + V_T^n + \frac{2\Delta t}{C_{ext}}\sum_{i=1}^{n} I_i \end{bmatrix} \tag{15}$$

NEWTON - RAPHSON METHOD

Due to the nonlinearity of the $\nu[S]$ matrix, the finite difference system of equations must be solved using a nonlinear equation solution technique such as the Newton-Raphson method. The Newton-Raphson method is used to find equilibrium at each time step. The method is shown in the following equations:

$$\left[\frac{\partial \Psi}{\partial Var}\right]\{\Delta Var\} = \{-\Psi\} \tag{16a}$$

$$\{Var\}_{i+1} = \{Var\}_i + \{\Delta Var\} \tag{16b}$$

Where $\{\Psi\}$ is the nonlinear homogeneous equation to be solved, $\left[\frac{\partial \Psi}{\partial Var}\right]$ is the assembled Jacobian matrix rendered symmetric by algebraic manipulation of equation (15), $\{Var\}_i$ is a vector of solution variables from the previous iteration, $\{Var\}_{i+1}$ is a vector of solution variables at the new iteration and $\{\Delta Var\}$ is a vector of corrections.

The Newton-Raphson method requires repeated inversion of the nonlinear Jacobian matrix. Since the Jacobian is not positive definite, a complex math "skyline" solver was used for inversion. During each iteration the ΔVar is solved for and used to update the prediction for the unknown variables.

TORQUE

Motor torque computation using finite element methods commonly relies either on the use of the Maxwell stress tensor or the virtual work principle. The stress tensor method requires several layers of air gap elements in order to obtain accurate values of the tangential flux density. The virtual work implementation normally requires two finite element solutions whose meshes are displaced a small rotation from each other. A more elegant virtual work method was developed by Coulomb and Meiner [10]. Their method requires only a single layer of elements in the air gap and one finite element solution at each time step. The magnetic energy expression is differentiated mathematically with respect to rotation before integration over the solution space and results in the following equation for the torque contribution per unit depth of each virtually distorted element in the air gap:

$$Te = -\nu_a \left[B_X \frac{d}{d\theta}\left[\sum_{i=1}^{n} \frac{dN_i}{dY} A_i \right] + B_Y \frac{d}{d\theta}\left[\sum_{i=1}^{n} \frac{dN_i}{dX} A_i \right] \right] A_e - \left(\frac{\nu_a}{2}\right)\left[\frac{B^2}{|J|} \frac{d|J|}{d\theta} \right] A_e \qquad (17)$$

Where ν_a is the reluctivity of air, B_X, B_Y are the X and Y flux densities, θ is angular rotation, B^2 is flux density squared, A_e is the element area, $\frac{dN_i}{dY}$, $\frac{dN_i}{dX}$ are derivatives of the shape functions N_i, A_i are nodal vector potentials and n is the number of nodes in the element. Additional details of the method can be found in [10] and [12].

RESULTS

Transformer

For three reasons a transformer was selected as a model to test the computer simulation. First, a transformer is similiar to an induction motor at standstill. Therefore the generated code would be directly applicable to a motor. Second, an isolation transformer of known contruction details was available for experimental verification. Third, the transformer lends itself to a simple mesh which can be easily modified or refined as required. The transformer was a 1.2 KVA, 120 Vac, 60 hertz model with a turns ratio of 1.1 (secondary to primary) and constructed of Arnold Technologies, Inc. M-22 steel. B-H points for the steel were selected from a published curve and a ν-versus-B^2 curve was fit using cubic splines [11]. The finite element grid for one-quarter of the transformer consisted of 216 triangles and 125 nodes and the time step used was one-sixtieth of a second. Approximations for the end leakage reactances were obtained from no-load and shorted-secondary tests. The transformer model was tested under three conditions: at no-load (i.e., with secondary winding open-circuited) for computation of the magnetizing current; with shorted-secondary to predict induced voltages and currents; and with a purely capacitive secondary load. A ramped sinusoidal voltage was applied to the model to minimize the startup transient of the solution, permitting steady state to be achieved in about 2-1/2 electrical cycles. Figure 1 shows steady-state computed and experimental results for the magnetizing current of the transformer. Differences in the current waveforms are due to hysteresis effects which are not modeled. The experimental and calculated RMS values of magnetizing current are 0.84 and 0.73 amps, respectively. In the shorted-secondary test, a voltage of 3.87 volts RMS was applied. The experimental primary and secondary currents are 11.5 and 10.6 amps; calculated values are 11.5 and 10.4 amps. These results demonstrate that the method of calculating induced voltages and currents is valid.

The most interesting results on the transformer were obtained using a capacitive secondary load of 25 microfarads. Figures 2 and 3 show the primary and secondary currents for the transformer. A pronounced second harmonic caused by resonance occurs in the primary current and is properly modeled. Surprisingly, secondary current remains essentially sinusoidal and is also modeled well. A summary of the experimental and modeled results for the transformer for the three load cases is given in Table 1.

Table 1. Transformer - Three Load Cases

Load Condition	Input Voltage (Volts)	RMS Current (Amps)				RMS Output Voltage (Volts)	
		Predicted		Measured		Predicted	Measured
		Prim.	Sec.	Prim.	Sec.		
No Load	120	0.84	-	0.73	-	131.9	132
Shorted Sec.	3.87	11.5	10.6	11.5	10.4	-	-
25 Mfd Cap.	120	0.83	1.24	0.83	1.25	130	132

AC Induction Motor - Locked Rotor

A two-pole permanent-split-capacitor motor was also modeled. The stator has 24 slots and the rotor 34 bars. A finite element grid composed of 3464 triangles and 1761 nodes was used for the model. The input for the model was again a ramped sine wave voltage with time steps of one-sixtieth of a second. An outline of the motor lamination and resulting vector potential contours (flux lines) is shown in Figure 4. For reference, the main winding axis is located along the horizontal and the auxiliary winding axis along the vertical. The vector potential contours are shown at one instant in time for the locked rotor condition. A series of figures over one electrical cycle would show the contours rotating and changing in magnitude as the magnetic field revolves within the motor. The plotted vector potential is the resultant of both winding currents and currents induced in the rotor.

AC Induction Motor - Moving Rotor

The final step in code development was the creation of a time-dependent mesh to permit the rotor to rotate and to be automatically reconnected to the stator through the airgap mesh. Because the rotor nodes are moving in their own coordinate system, it is unnecessary to add the speed voltage term to Equation (8) with this technique. The solution procedure is conceptually simple but involves much bookkeeping. At each time step the nodes in the rotor are incremented through a small angle, the airgap elements between the stator and rotor reconnected, the model bandwidth minimized, electric circuit equations added to the matrices and a Newton-Raphson iteration performed. Much smaller time steps were required than for the transformer or motor at locked rotor conditions. Steps corresponding to one or two mechanical degrees were required both for computational stability and for sufficient definition in plotted results. The mesh, nodal results (i.e., vector potential and vector potential derivatives), voltages across windings and winding and rotorbar currents at each time step after steady state is reached are saved for post-processing.

It is again noted that the solution of equation (15) is time-dependent in nature and several electrical cycles must be solved to allow any startup transients to die out. Our procedure was to set rotor rotation at the desired speed and then apply a ramped sinusoidal voltage to the motor windings for the first two or three electrical line cycles. Seven to ten additional line cycles were then required to reach a quasi-steady state solution, that is, where each succeeding cycle was approximately the same as the previous cycle. Cycles will not repeat exactly due to motor slip when running at other than synchronous speed.

Post-processing for each time step consists of calculation of the magnetic field intensity, eddy currents in rotor bars, motor torque and an instantaneous power balance for the motor. The power balance includes the rate of change of magnetic energy in the finite elements, the rates of change of energy in circuit inductances and capacitor, winding I-squared-R losses and eddy current losses in rotorbars, the sum of which must equal the instantaneous input line power. Power balances within a few percent were achieved.

Motor torque at each time step is computed using the virtual work principle described previously. In contrast to Strangas and Theis [6], who used an airgap mesh composed of elements which could stretch elastically, the authors found it necessary to "lockstep" the rotor to prevent element distortion during rotation. Element distortion drastically affects the magnetic energy in the element as the element area changes and prevents accurate torque calculation. The "lockstepping" technique consists of meshing the airgap with uniform elements and rotating the mesh an integral number of airgap elements at each time step.

Calculated results from the model are instantaneous values of flux density, rotor bar currents, torques, line, main and auxiliary currents and voltages, and many others. Air gap flux densities can be plotted to check winding distributions, torques examined for alternating components, eddy current losses checked in rotor bars, etc. A plot of input power and motor output torque is shown in Figure 5 which clearly shows the alternating torque characteristic of single-phase motors. Table 2 shows representative time-averaged results together with dynamometer data where available.

Table 2. PSC Induction Motor - 230 Vac Line Volts

	3600 RPM (Synchronous)		3500 RPM (Full Load)		2900 RPM (Breakdown.)		Locked Rotor	
	Measured	Predicted	Measured	Predicted	Measured	Predicted	Measured	Predicted
Torque*	-2.1	-2.1	67	67	158	156	13-15	11.7
Line Amps	1.26	1.36	10.2	10.3	-	41.9	58-62	60.2
Line Watts	172	150	2,363	2,365	-	8,113	-	8,521
Main Amps	5.07	5.14	8.1	8.1	-	41.8	-	62.7
Main Watts	-690	-711	1,575	1,561	-	7,711	-	8,466
Aux Amps	5.02	5.24	4.4	4.6	-	2.87	3.23	3.33
Aux Watts	860	861	794	804	-	402	-	55
Aux Volts	280	-	257	262	-	141	-	23
Cap. Volts	377	397	333	343	-	214	245	250

* Torque in Ounce-Feet (11.8 oz-ft = 1 nt-m)

The modeling technique inherently accounts for motor leakage reactances such as slot, belt and zig-zag leakages [1], but not end or skew leakage, which must be included in the circuit equations. Iron losses must also be separately included in the model, but are easier to estimate with the more complete knowledge of the magnetic field quantities. Friction and windage losses must also be separately considered and corrections made to calculated currents.

CONCLUSIONS

A method of modeling magnetic devices using a two-dimensional finite element approach coupled with electric circuit equations has been developed. The finite element solution yields the time-varying magnetic field solution within the device and the circuit equations account for both end effects and external circuit elements. The governing equations have been cast in a form that allows the forcing functions to be time-varying terminal voltages. Results give not only the magnetic field solutions for the entire device, but also permit calculation of eddy currents in conductors. Another result of the solution technique is that magnetic flux density variation is calculated in every element of the mesh. Both major and minor flux reversals are modeled which permits core losses to be estimated. Experimental and predicted results for a transformer and a permanent-split-capacitor induction motor both at standstill and with moving rotor have been presented. The model and experiment are in excellent agreement in all cases.

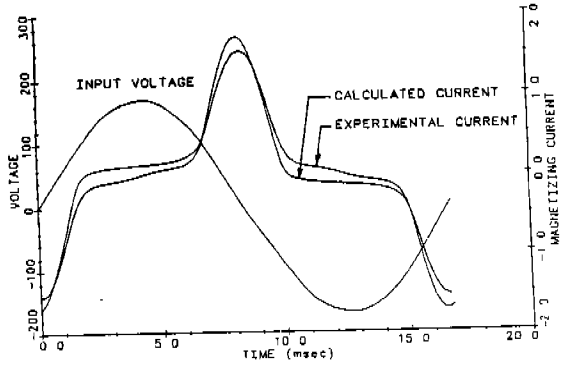

Figure 1. Transformer input voltage and magnetizing current versus time.

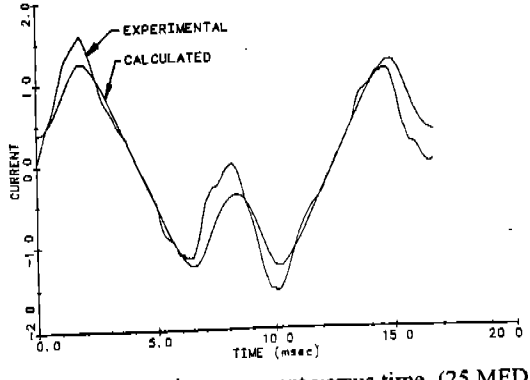

Figure 2. Transformer primary current versus time (25 MFD Capacitor).

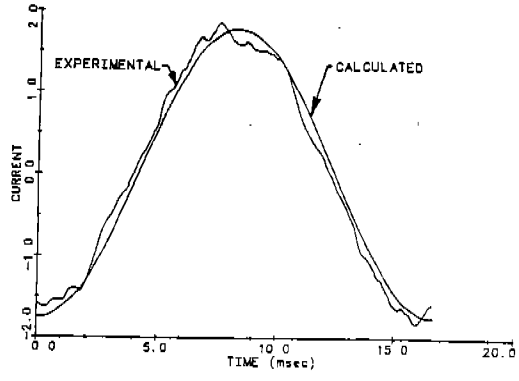

Figure 3. Transformer secondary current versus time (25 MFD Capacitor).

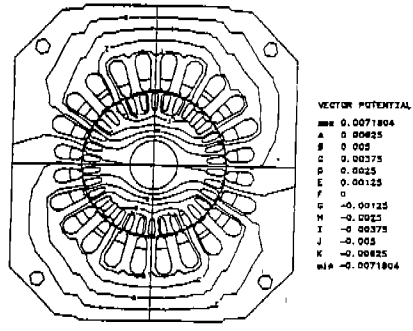

Figure 4. PSC induction motor vector potential contour plot.

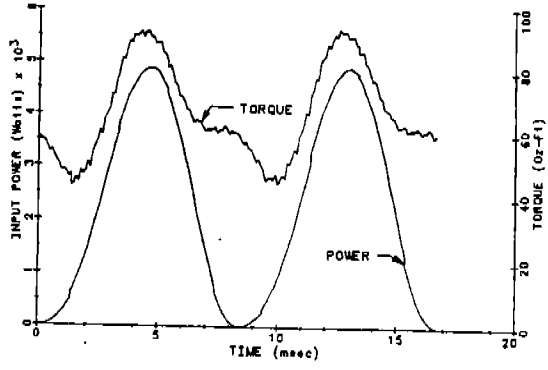

Figure 5. Calculated torque and power input for PSC induction motor.

REFERENCES

[1] C.G.Veinott, Theory and Design of Small Induction Motors, McGraw-Hill, New York, N.Y., 1959.

[2] M.V.K. Chari and P. Silvester, "Finite-Element Analysis of Magnetically Saturated D-C Machines," IEEE PES, Paper 71 TP3-PWR, 1971.

[3] S.R.H. Hoole, Computer-Aided Analysis and Design of Electromagnetic Devices, Elsevier, New York, N.Y., 1989.

[4] S. C. Tandon, A. F. Armor, and M.V.K. Chari, "Nonlinear Transient Finite Element Field Computation of Electrical Machines and Devices," IEEE Trans. PAS, Vol. 102 May 1983, pp. 1089-1096.

[5] P.G. Potter and G.K. Cambrell, "A Combined Finite Element and Loop Analysis For Nonlinearly Interacting Magnetic Fields and Circuits," IEEE Trans. MAG, Vol 19, No. 6, Nov. 1983, pp. 2352-2355.

[6] E.G. Strangas and K.R. Theis, "Shaded Pole Motor Design and Evaluation Using Coupled Field and Circuit Equations," IEEE Trans. MAG, Vol. 21, No. 5 Sept. 1985, pp. 1880-1882.

[7] O.C. Zienkiewicz, The Finite Element Method, Third Ed., McGraw-Hill, (UK), Berk shire, England, 1977.

[8] K.J. Bathe and E.L.Wilson, Numerical Methods In Finite Element Analysis, Prentice-Hall, Englewood, N.J., 1976.

[9] J. Crank and P. Nicholson, "A Practical Method for Numerical Solutions of Partial Differential Equations of Heat Conduction Type," Proc. Caub. Phil Solc. 43, 1947, pp.50-67.

[10] J.L. Coulomb and G. Meunier, "Finite Element Implementation of Virtual Work Principle For Magnetic or Electric Force and Torque Computation," IEEE Trans. MAG, Vol. 20, No. 5, Sept. 1984, pp. 1894-1896.

[11] P. Silvester, H.S. Cabayan and B.T. Browne, "Efficient Techniques for Finite Ele ment Analysis of Electric Machines," IEEE PES, Paper T73 301-0, 1973.

[12] L.W.Marriott and G.C.Griner, "Induction Motor Modeling Using Coupled Magnetic Field and Electrical Circuit Equations," Proc. of the 42nd Annual International Appliance Technical Conference, May 21-22, 1991, pp. 567-578.